ADVANCED ELECTRONIC MATERIALS

Supporting Information

for *Adv. Electron. Mater.,* DOI: 10.1002/aelm.202100970

Resistivity Scaling Transition in Ultrathin Metal Film at Critical Thickness and Its Implication for the Transparent Conductor Applications

*Yong-Bum Park, Changyeong Jeong, and L. Jay Guo**

Supporting Information for

Resistivity scaling transition in ultrathin metal film at critical thickness and its implication for the transparent conductor applications

Yong-Bum Park, Changyeong Jeong, and L. Jay Guo*

Department of Electrical Engineering and Computer Science, University of Michigan, Ann Arbor, MI 48109, USA

** Corresponding author. Telephone: 1-734-647-7718; Fax: 1-734-763-9324; Email: guo@umich.edu*

Table of contents

SECTION 1 | Universality of double-slope in thin Ag film

SECTION 2 | Physical parameters of ultrathin Ag (Cu) film

SECTION 3 | Optimization of fitting parameters in size effect models

SECTION 4 | Parameter extraction for general effective media (GEM) model

SECTION 5 | Percolation model and effective medium approximation models

SECTION 6 | Justification of extended GEM model

SECTION 7 | Ag (Cu) film's dielectric function near metal-insulator transition

SECTION 8 | Electrical properties of Ag (Cu) film near the critical thickness

SECTION 9 | Film's electrical hysteresis over time

SECTION 1 | Universality of double-slope in thin Ag film

As the thin metal film's resistivity is often described to have an exponential decay function of the thickness, it would be useful to plot it under log-log scale. To test if the double-sloped behavior is specific to the copper (Cu)-seeded silver (Ag) film named as Ag (Cu) film, other type of widely used seed layer germanium (Ge) or even Ag film without any seed layer. **Figure S1a** and **b** shows the log-log plot of resistivity-thickness ($\rho - d$) of Ag film with Ge-seed

or without any, respectively. What this show is regardless of the type of nucleation layer or without this layer, Ag film's transport behavior has two distinct linear regimes in log-log plot.

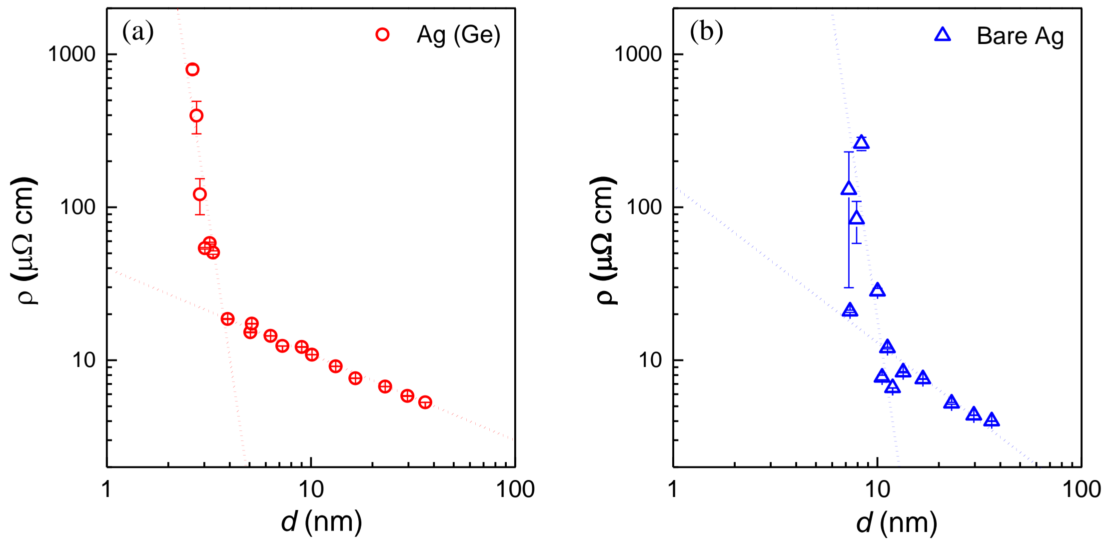

Figure S1 | (a) Log-Log resistivity ρ versus thickness d plots of (a) Ge-Ag and (b) bare Ag film. The open symbols are the measured data while dotted lines extrapolating double-slope behavior of resistivity scaling are not based on any physical model.

SECTION 2 | Physical parameters of ultrathin Ag (Cu) film

Ultrathin Ag (Cu) film's physical properties like surface roughness, grain size, and metal fraction of film were extracted from the measured data to be used as physical parameters in size effect model and generalized effective medium model. The film's root-mean-square (RMS) surface roughness values were obtained from atomic-force-microscopy (AFM, Bruker ICON) analysis under the tapping mode, in which the extracted film's average RMS roughness value was used as a parameter in surface roughness models. First, **Figure S2a** is the plot of Ag (Cu) film's root-mean-square (RMS) surface roughness as a function of film's effective thickness d_{eff}. The film maintains a relatively smooth surface for thickness range from 4 to 8 nm but then rapidly increases below 4 nm due to the inhomogeneous film property. Next, X-ray diffractometer (XRD, Rigaku SmartLab) data was obtained using Cu-Kα radiation and estimated grain size (in thickness direction) was extracted using Scherrer equation for varying Ag thickness as shown in **Figure S2b** and **c**. We assumed that lateral grain size proportionally grows along with the longitudinal size. As the crystallite grain size extracted from XRD is only good to show

the trend while it may not represent the actual size, $d \sim D$ proportionality relation was used as an approximation for the D in M-S model [1].

For the calculation of size effect models, bulk resistivity of ρ_i = 1.59 μΩ·cm and electron mean free path of l_0 = 53 nm was used for silver film.[2] Surface roughness models by Soffer[3] and Namba[4] were adopted to calculate the resistivity. Ag film's RMS surface roughness values of R_a = 0.263 nm (Figure S2a) was used to extract physically meaningful r_1 and h values for these models. The extracted roughness amplitude was $r_1 = h = \sqrt{2} \times R_a = 0.37$ nm. r_2 of 0.71 nm was used to reflect the possible roughness caused by the seed layer. For M-S model, the grain size D is set equal to the film's thickness d, which is a reasonable approximation for physical vapor deposited metal films within relatively thin regime. [1, 5]

Lastly, to extract metal fraction (projected area) ϕ of Ag (Cu) film as a function of film's d_{eff}, multiple of top-down TEM and scanning transmission electron microscope (STEM) images were extracted for each thickness. Samples were prepared on a TEM grid with same imaging condition as described on main text. STEM imaging was conducted using a JEOL 3100R05 double-corrected S/TEM operated at 300 kV. High-angle annular dark-field images were acquired in a collection range of 59–200 mrad with a probe convergence angle of 22 mrad. **Figure S2d-h** shows the selected TEM images for each thickness (d_{eff} from 2.0 - 8.5 nm) after performing image processing to calculate the void area. Same cutoff condition was applied for void calculation for all the images. The region that appears to be bright in TEM images are voids whereas that appear as dark spots in the STEM image (inset of Figure S2f) are voids. To reduce the measurement error, ϕ values were averaged over at least 8 different TEM images from different spots and was cross-checked with that obtained from STEM image for each thickness. For further information, original images before image processing have been provided in **Figure S2i-m**. Also, **Figure S3a** and **b** are added to further aid Ag (Cu) film's crystalline behavior under TEM and surface morphology under AFM, respectively.

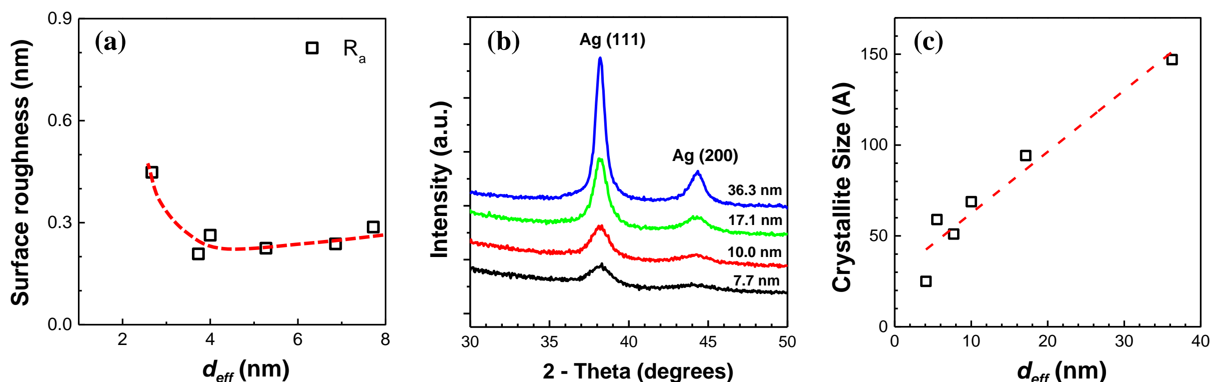

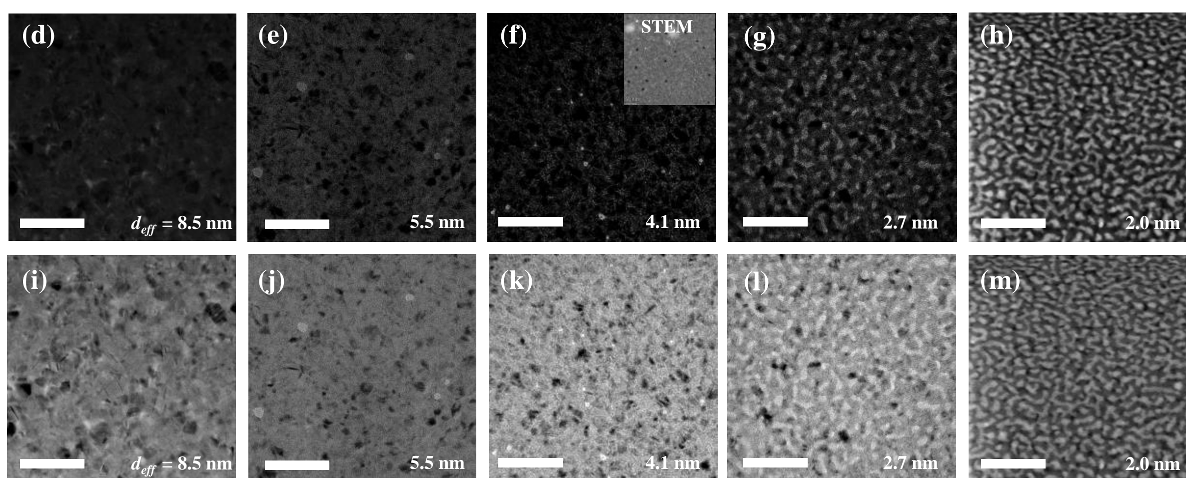

Figure S2 | Ag (Cu) film's (a) RMS surface roughness values as a function of d_{eff}. (b) XRD intensity curve over 2- theta for different film thickness. (c) Extracted film's crystallite grain size as a function of d_{eff} showing linear relationship. Inset figure is TEM image of the film with 10 nm of thickness, which show approximate grain sizes in the range of *D* ~ 10 nm. Top-down TEM images after image processing of Ag (Cu) film with effective thickness of (d) 8.5 nm, (e) 5.5 nm, (f) 4.1 nm, (g) 2.7 nm, and (h) 2.0 nm. Similarly, original TEM images of Ag (Cu) film with effective thickness of (i) 8.5 nm, (j) 5.5 nm, (k) 4.1 nm, (l) 2.7 nm, and (m) 2.0 nm All images have scale bar of 50 nm. Inset of (f) is the STEM image taken as an example where black dots show void areas.

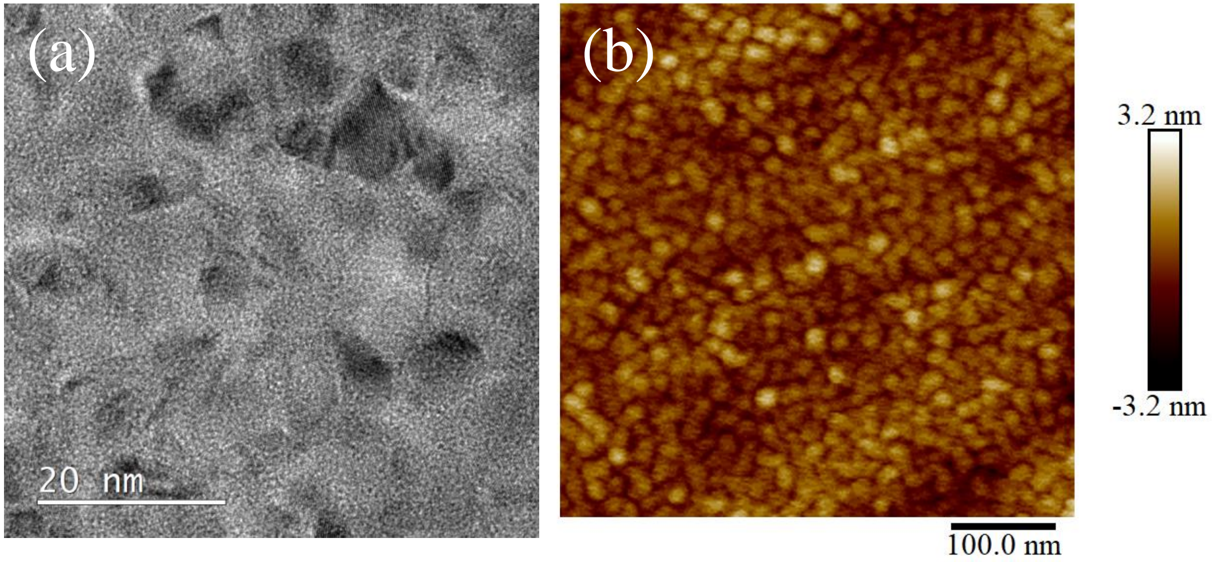

Figure S3 | (a) TEM bright field image of Ag (Cu) film with thickness of 10 nm (b) AFM image of surface morphology of Ag (Cu) film with effective thickness of 7 nm.

SECTION 3 | Optimization of fitting parameters in size effect models

Surface versus Gain boundary scattering in ultrathin Ag (Cu) film: This section exploits the comparison of surface and grain boundary scattering models to describe the experimental resistivity data of Ag (Cu) film where ρ versus d is plotted in linear-linear (**Figure S4a**) and log-log plots (**Figure S4b**). The empirical Ag (Cu) film's resistivity data are plotted in symbol and modeled data are plotted in lines. For surface scattering model, the effect of varying p value from 0 to 1 in Fuchs-Sondheimer (F-S)'s surface scattering model[6] is studied. For a given specularity parameter p, resistivity increases as the film thickness d decreases to a level comparable or below electron mean free path l_0. This trend is more obvious as p is decreased, which can be intuitively explained from F-S model. One thing to note however, is that F-S model severely underestimates the resistivity, even for the case of totally diffusive scattering ($p = 0$). As pointed out earlier, this may be attributed to the actual film not being single crystalline nor having atomically flat surface. Next, grain boundary scattering effect on the resistivity of thin film was studied using Mayadas-Shatzkes (M-S) model[1] by sweeping the reflection coefficient R value from lower limit of 0 to upper limit of 1. As mentioned previously, the grain size is assumed to be proportional to the film thickness, which is typical for thin metal film growth. It is evident that the resistivity is a very strong function of R unlike F-S model especially at a region of

extremely thin regime as shown in Figure S4a. On the surface, M-S model with reflection coefficient of approximately R ~ 0.4 (40% probability of electron wave being reflected at the grain boundary) seems to well describes the resistivity scaling of measured data compared to F-S model. This statement is rational because most metal films grown in PVD system are polycrystalline or amorphous in nature. However, when plotting ρ - d in log-log scale as in Figure S4b, there is a slight discrepancy between the M-S model and the experimental result throughout the entire thickness regime even when excluding thickness below 5 nm. This reasonably shows that the empirical resistivity cannot be explained by either one of the models.

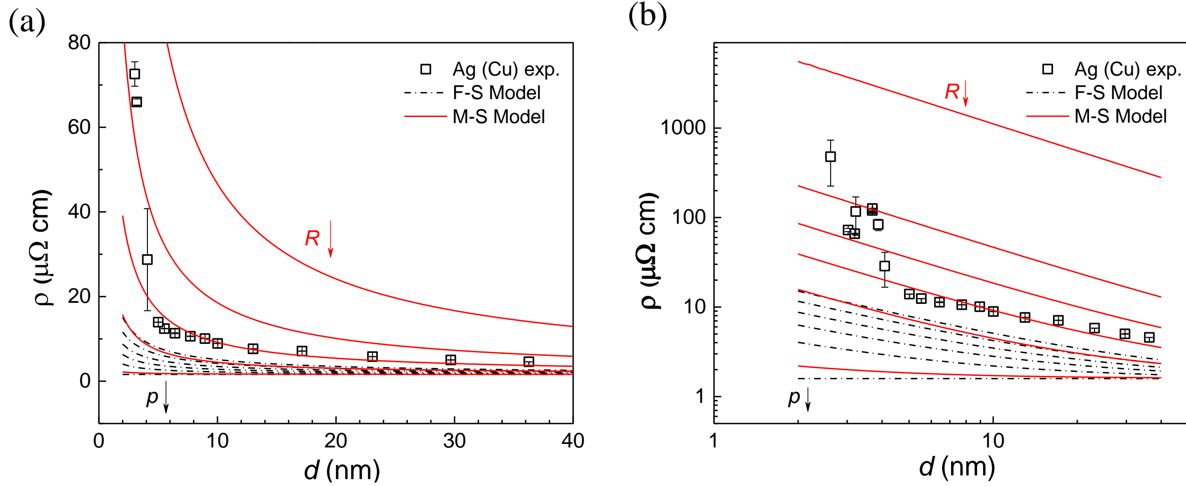

Figure S4 | Theoretically calculated ρ - d plot in (a) linear-linear and (b) log-log scale of Ag (Cu) thin film using surface (F-S) or grain boundary (M-S) scattering models each model with varying specularity parameter p and reflection coefficient R, respectively. The open symbols are the measured data. F-S and M-S models are plotted in dotted-black and red-solid lines, respectively. Theoretical values calculated for sweeping parameters where arrows indicate the direction of parameters (with ranges $0 \leq p \leq 1$ and $0 < R < 1$) in decreasing order.

Fitting optimization with Matthiessen's rule: In thin metal film, both surface (or roughness) and grain boundary scattering would take role in decreasing the conductivity where the rate determining step would be the event that has the highest rate. To determine which combination of models best describe the experimental resistivity data, the deviation δ of theoretical resistivity (ρ_{theory}) from experimental resistivity (ρ_{exp}) was quantified by the following equation:

$$\delta = \sum_d \left\{ \left(\rho_{theory}(d) - \rho_{exp}(d) \right) \times d \right\}^2 \qquad \text{(S1)}$$

where the deviation of resistivity at each thickness was weighed by d to depreciate the large resistivity deviation at lower thickness. For each combination of theoretical models, optimum fitting parameters that minimizes δ were selected to best represent experimental data.

For the combination of models involving one or two fitting parameters, 1-dimensional plot or 2-dimensional plot of deviation was calculated for the entire range of parameters. Optimum sets of fitting parameters (p or R) were selected that gives lowest deivation values. Color map showing the log of *devation*) was used to find optimum parameters of models involving two fitting parameters while 1-dimensional curve was used to find the optimum parameter involving one fitting parameter. Example of optimization of two fitting parameters is shown in **Figure S5a**, in which this map was for the total resistivity ρ_{total} calculated by the summation of Namba and M-S models ($\rho_{total} = \rho_{Namba} + \rho_{MS} - \rho_i$). Fitting parameters of p for Namba model and R for M-S models were swept for its entire range from 0 to 1 and the best fitting was found at p = 0.1 and R = 0.2. All combinations of surface and grain boundary scattering models are plotted in **Figure S5b**. For ρ_{FS}, even when setting p = 0.0 (completely diffusive scattering at the surface), the model significantly underestimates the resistivity for the entire range. Such behavior is very similar to the resistivity predicted by other surface scattering models. This further shows that a surface scattering contribution becomes quite small especially when the film's thickness is thin regime below 40 nm. Among the surface (roughness) scattering models, Namba's model shows the largest increase in resistivity as film thickness decreases, which may be originating from the strong dependence on resistivity on sinusoidal representation of surface roughness. Portion of surface scattering induced by grain boundary scattering described in MSS model is quite insignificant (p = 0.7, R = 0.42). This is because the interaction between the two becomes substantial only at low temperature,[7] which is why resistivity described by MSS model shows similar behavior as grain-boundary-only MS model (R = 0.44). Overall, the decoupling of surface and grain boundary scattering by using Matthiessen's rule best explains our empirical data which is consistent with other works. [7, 8]

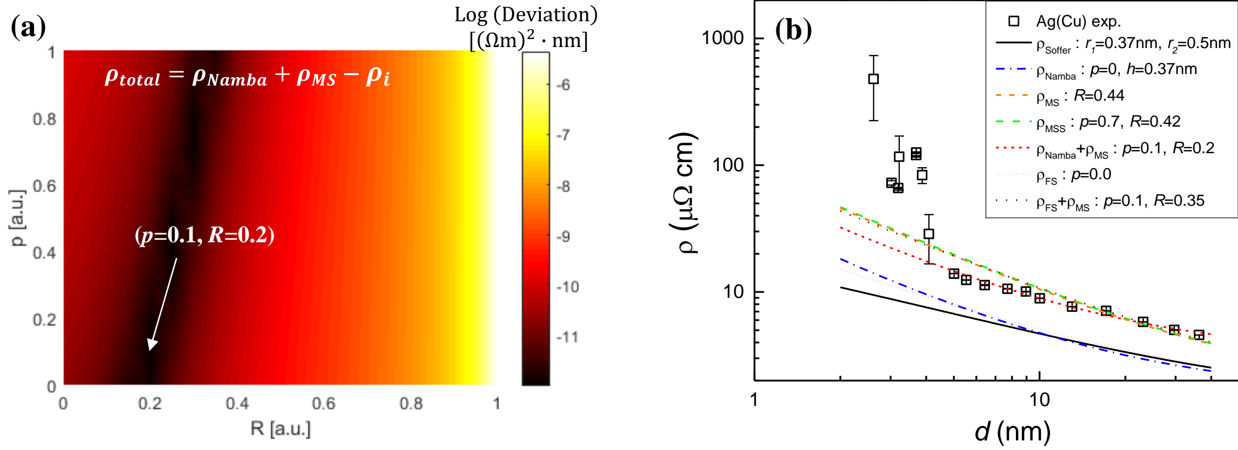

Figure S5 | (a) Colormap of deviation [Equation S1] in theoretical model (Namba + M-S models) from experimental data involving two parameters, p and R where optimum point is at $p = 0.1$ and $R = 0.2$. Colormap scale is plotted in log scale. (b) Comparison of resistivity data predicted by all the combinations of surface or grain boundary models. Data in symbol is measured data while that in lines are calculated from a single or sets of models.

SECTION 4 | Parameter extraction for general effective media (GEM) model

There are few parameters that need to be extracted to see if GEM model can express the experimental resistivity scaling for extremely thin regime. First, percolation threshold fraction ϕ_c and critical exponent of conductivity t need to be determined. To determine ϕ_c and t, the data have been fit to the power law:

$$\rho \sim \rho_0[(\phi - \phi_c)/(1-\phi_c)]^{-t} \quad \text{(S2)}$$

where ρ_0 is the resistivity scaling factor. The Metal fraction in each metal films was extracted from TEM images (Figure S2d–f). The negative of the slope in the inset figure of **Figure S6a** is the critical exponent of conductivity t,[9] which was extracted as $t = 3.06 \pm 0.2$, with a percolation threshold value ϕ_c of 0.59 and resistivity factor ρ_0 of 7.66 μΩ cm (value at which film becomes completely free of voids). The R-Square value for the fit is 0.9932, indicating a reasonable fit. It has been verified experimentally that the critical exponent of a metal-insulator composite follows a three-dimensional network with theoretical universal value of $t = 2$ [10, 11] although non-universal behavior of values close to 3 have been commonly observed,[9, 12] which is explained in terms of the mean-field behavior.[13] For our film's case, the critical exponent of conductivity follows more of the mean-field value that may be affected by the non-uniform size

distribution of metal clusters. In case of percolation threshold ϕ_c, a theoretically calculated value of percolation for a disk shape (which may resemble a typical metal cluster) is 0.6763.[14] However, wide range of values from 0.47[15] to 0.63[16] were experimentally reported for metal films. For our film's case, with ϕ_c= 0.59 and t = 3.06, the electrical percolation model [10] of $\rho/\rho_0 \sim (\phi - \phi_c)^{-t}$ for $\phi > \phi_c$ and $\rho/\rho_1 \sim (\phi_c - \phi)^s$ for $\phi < \phi_c$ well represents the experimental resistivity data as shown in Figure S6a. Here, critical exponent value s at lower metal fraction of s = 1 and metal-insulator resistivity ratio of ρ_0/ρ_1 = 10^8 was used.[10] As a further evidence, we observed the real part of the optical dielectric function changing its sign from negative to positive in the vicinity of ϕ_c= 0.59 (which will be discussed in **Figure S9**) which is indicative of metal-to-insulator transition.[11] From these results, the extracted values of ϕ_c and t best represent the physical nature of our film and so are reasonable values to use for GEM model in representing percolation effect. Next, a relationship between the effective thickness d_{eff} versus metal fraction ϕ is needed to use GEM model to express resistivity as a function of thickness. Although effective thickness may be more appropriate to use for inhomogeneous type of film but both average and effective thickness hold identical meaning and so will be interchangeably used to represent the film's thickness of entire thickness range throughout the text. **Figure S6b** shows the empirical relationship obtained for effective thickness versus metal fraction using logistic function which is a reasonable approximation as the metal fraction will saturate to either 0 or 1 as film thickness goes to lower or upper extreme.

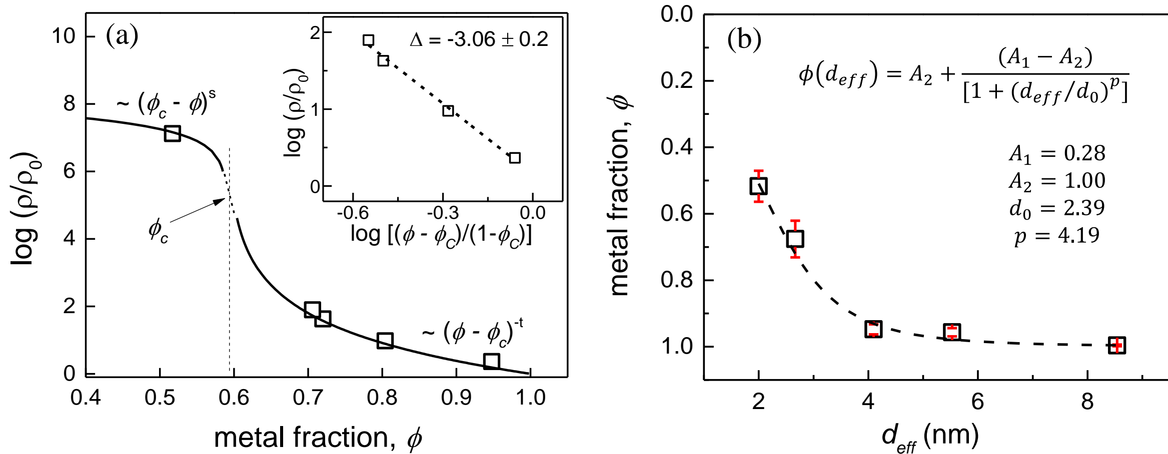

Figure S6 | (a) Log plot of normalized resistivity ρ/ρ_0 as a function of metal fraction for measured and theory. Percolation theory of conductivity with $\rho/\rho_0 = A(\phi - \phi_c)^{-t}$ for $\phi > \phi_c$ and $\rho/\rho_1 =$

$B(\phi_c - \phi)^s$ for $\phi < \phi_c$ was used as a model for theoretical calculation. Percolation threshold ϕ_c of 0.59 (indicated as dotted line), critical exponent values of t and s of 3.06 and 1.0, respectively, metal-insulator resistivity ratio of $\rho_0/\rho_1 = 10^8$ was used where resistivity scaling factors ρ_0 and ρ_1 are the resistivity of metal and insulator, respectively. Proportionality factor of A = 0.07 and B = 2 were used. Inset graph shows a plot of ρ/ρ_0 as a function of $(\phi - \phi_c)/(1 - \phi_c)$ in log-log scale where the negative of the slope Δ represent t found here as 3.06 $\pm$ 0.2. (b) The measured metal fraction ϕ of Ag (Cu) film as a function of film's effective thickness d_{eff} shown as a symbol. Its empirical relationship was extracted using logic function plotted in dotted line (equation in the inset).

SECTION 5 | Percolation model and effective medium approximation models

In this section, effective medium and percolation models will be compared with GEM to see which model best describe the resistivity ρ scaling near percolation threshold. First, we begin with electrical percolation model ($\rho_{percolation}$) approaching from higher metal fraction ϕ: [10]

$$\rho_{percolation}/\rho_0 \sim (\phi - \phi_c)^{-t} \quad \text{(S3)}$$

where ρ_0 is the resistivity scaling factor, ϕ_c is the percolation threshold fraction, t is the critical exponent of conductivity. This electrical percolation theory which uses power law to describe the transition of conductivity applies only to near the conductor-insulator transition region. Next, we look into the effective medium approximation (EMA) by Landauer model (ρ_{EMA}) which describes the electrical conduction in inhomogeneous medium[17] given as:

$$\rho_{EMA}/\rho_0 = (1 - \phi_c)/(\phi - \phi_c) \quad \text{(S4)}$$

For parameters like ϕ_c, ρ_0, and t, values were used identical to what was used in SECION 4. Also, empirical relationship between d_{eff} and ϕ described in Figure S6b was used to transform these models into d_{eff} domain. The results from all four models are plotted in **Figure S7**. From this result, extended GEM best describes the resistivity scaling near or below 5 nm compared to percolation model or EMA model. In case of percolation model, the power-law nature of the model gives good approximation near the percolation threshold of 2.4 nm. However, the resistivity scaling factor to the power of t prevents it from converging to ρ_0 at high metal fraction. Proportionality constant can be used to better fit the data as shown in orange dotted line (i.e. A=0.07 as in SECTION 4) although this points out another limitation of the model relying on arbitrary fitting parameter. For the case of EMA model, despite its convergence to ρ_0 at larger d_{eff}, it gives poor approximation near the percolation threshold thickness. GEM model which

excludes the size effect theory, better represent the overall resistivity scaling compared to former two models but still showing a level of insufficiency (due to the absence of size effect theory). By considering size effect into GEM, extended GEM shows good prediction to the experimental data which is a more physically correct and relevant picture for our ultrathin Ag (Cu) film.

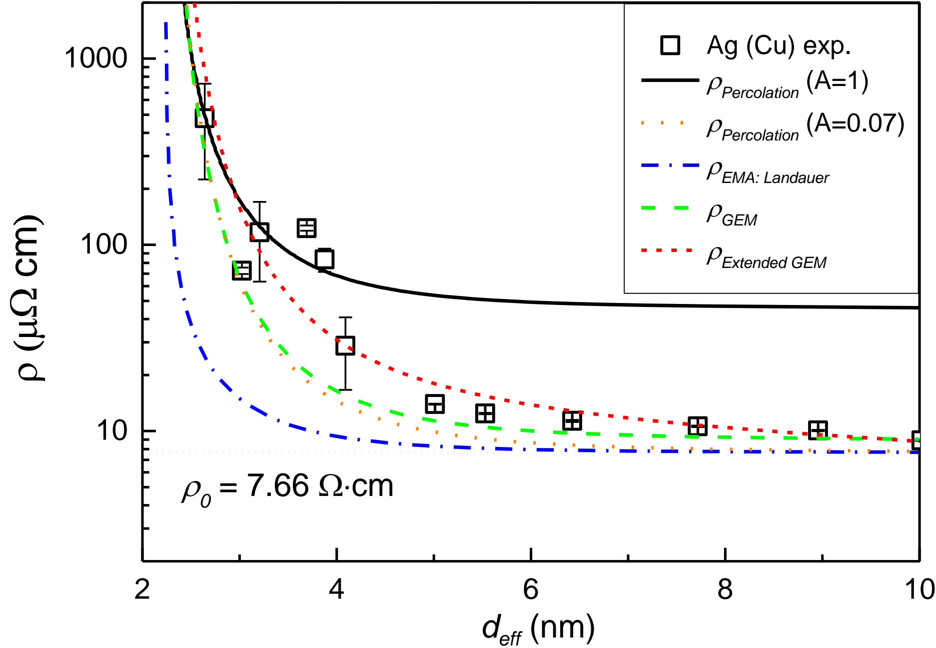

Figure S7 | ρ - d_{eff} plot from percolation model ($\rho_{percolation}$, Equation S3), Landauer model (ρ_{EMA}, Equation S4), GEM model [ρ_{GEM}, Equation 2 from the main text with constant ρ_0] and extended GEM model [$\rho_{ext.GEM}$, Equation 2 with ρ_0= ρ_{size}]. Grey horizontal line indicates bulk resistivity or resistivity factor with value of 7.66 Ω cm. Experimental resistivity values are plotted in symbol for reference.

SECTION 6 | Justification of extended GEM model

Using $\phi(d_{eff})$, ϕ_c, and t values, resistivity value from conventional GEM model with constant metal resistivity ($\rho_0 = 1/\sigma_0$ in **Equation 2** from the main text) denoted as ρ_{GEM} is plotted as blue dotted line in **Figure S8**. Percolation threshold ϕ_c of 0.59 which corresponds to d_{eff} = 2.4 nm is marked as a grey dotted vertical line in the figure. Despite the power law in GEM model allows rapid increase of resistivity in the proximity of percolation threshold ϕ_c (grey dashed line), the conventional GEM model alone is insufficient to accurately describe the resistivity at d_{eff} near 5 nm regime. The discrepancy between the model and the measured value remains even if the resistivity factor ρ_0 is set to a higher value. The discrepancy arises because

the model assumes a constant resistivity ($\rho_0 = 1/\sigma_0$) throughout the entire range of $\phi(d_{eff})$ which is incorrect as the scattering at grain boundary or surfaces still exist at this regime. In practice, size effect affects the scaling of resistivity as d_{eff} reduces, so the resistivity factor taken from bulk metal in GEM model (ρ_0) needs to be treated as a variable instead of constant value. To overcome this limitation, ρ_0 in the GEM model expressed by Equation 2, should be substituted by the size effect limited resistivity ρ_{size} to account for the actual resistivity of the metal phase. As discussed in the main text, we will refer to this slightly modified model as extended GEM model noted as $\rho_{ext.\ GEM}$. By considering the resistivity increase due to size effect theory, the GEM model can dynamically capture the change in resistivity as film size shrinks to a few nm regimes. This is important because the conduction of the electron at such thin regime cannot be described in a piecewise manner but two mechanisms are interlinked to determine the total resistivity. Therefore, representing resistivity factor as a function of film's thickness in GEM model should correctly depict the physical nature of the film. The result is plotted in Figure S8 with red short-dashed line showing surprisingly excellent fit for the experimental data through the entire thickness range including the $d_{eff} < 5$ nm regime. For the range of film thickness sufficiently large where the film is free of voids ($\phi = 1$), $\rho_{ext.\ GEM}$ naturally converges to ρ_{size}. As the scattering due to size effect theory directly influence the conduction within metal-insulator medium, these two events cannot be decoupled. Therefore, Matthiessen's rule is not applicable in this case but extended GEM model which couples size effect with GEM model is physically more relevant. This is verified by plotting the case of assuming Matthiessen's rule for contribution by GEM $\Delta\rho_{GEM}$ ($= \rho_{GEM} - \rho_0$) summing with ρ_{Size} as green dash-dot line in Figure S8 showing under-estimation of the resistivity in the d_{eff} slightly below 5 nm.

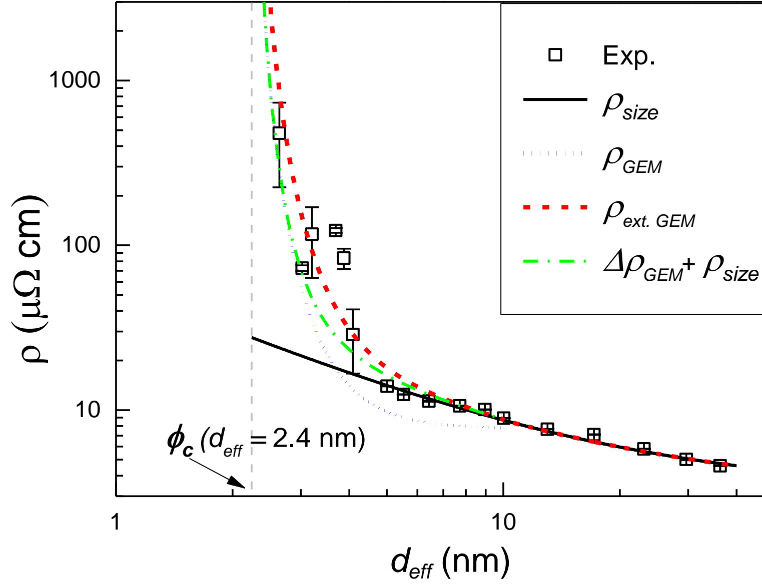

Figure S8 | Resistivity ρ of Ag (Cu) film as a function of film's effective thickness d_{eff}. The open symbols are experimental resistivity values and lines are calculated values from the theoretical models based on size effect (ρ_{size} [Equation 1], black solid line), GEM (ρ_{GEM} [Equation 2], blue dotted line), extended GEM ($\rho_{ext.GEM}$ [Equation 2 with replacing σ_0 with $\sigma_{size} = 1/\rho_{size}$], red dashed line), or applying Matthiessen's rule ($\Delta\rho_{GEM}+\rho_{size}$ [Equation 1 and 2], green dashed-dot line). Thickness that corresponds to the percolation threshold ϕ_c is shown as vertical grey dashed line for reference.

SECTION 7 | Ag (Cu) film's dielectric function near metal-insulator transition

Experimental dielectric function: Ag (Cu) film's measured real ε_1 and imaginary ε_2 part of dielectric function for different film thickness d_{eff} are shown in **Figure S9a** and **b**, respectively, plotted over wavelength range from 380 to 1500 nm. In case of ε_1, a clear trend is observed where the curve remains relatively unchanged at thickness above 5 nm but then starts to rapidly rise for d_{eff} below 4 nm. As a result of gradual increase in the inhomogeneity of metal film (metal-insulator composite), air voids in the film influence the overall ε_1 to lean toward positive values. Below percolation threshold thickness of 2.4 nm, transition of the film to dielectric-behavior is observed showing positive ε_1 values over the plotted wavelength range. The behavior of ε_2 is slightly more complex as it involves various loss mechanisms as a form of phonon or

plasmon but overall trend shows increase in the loss as film's thickness goes below 5 nm. Plotting ε_1 at 1500 nm of wavelength (near-infrared) as a function of metal fraction ϕ is plotted as symbol in Figure S9c. Modeling percolation behavior of metal-insulator transition near percolation threshold ϕ_c is plotted as dotted curve line by fitting $\varepsilon_1 \propto (d_0 - d)$ relationship [11]. Despite the rough estimate by the model, it shows a clear transition of ε_1 from negative to positive value near ϕ_c (=0.59, indicated as vertical black dotted line). This further verifies validity of extracted ϕ_c from electrical model discussed in Figure S6a.

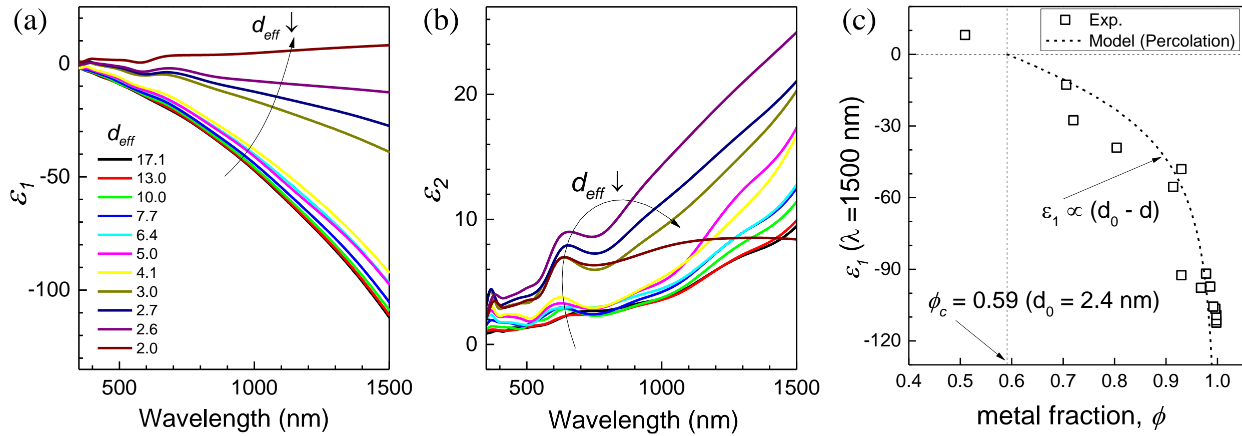

Figure S9 | (a) Real part ε_1 and (b) imaginary part ε_2 of Ag (Cu) film's dielectric function for different film thickness d_{eff}. Black arrows indicate the curve change behavior as decreasing d_{eff}. (c) Measured ε_1 (in symbol) at wavelength of 1500 nm as a function of film's metal fraction ϕ, where ϕ for a given film thickness was obtained from empirical relationship in Figure S6b. Modeled ε_1 (dashed line) using percolation model. Percolation threshold ϕ_c of 0.59 is indicated in vertical black dotted line. ϕ_c coincide with the metal fraction at which ε_1 crosses 0 indicative of metal-insulator transition.

Modeling of dielectric function for inhomogeneous medium: Dielectric function of Ag film at ultrathin regime was modeled using Bruggeman's effective medium theory (BEMT) to optically verify the inhomogeneous behavior of metal film near film thickness of 5 nm. According to BEMT, dielectric function of inhomogeneous metal film ε_{eff} can be solved by solving the following equation:[18]

$$f_m \cdot \frac{\varepsilon_m - \varepsilon_{eff}}{\varepsilon_{eff} + L(\varepsilon_m - \varepsilon_{eff})} + f_{air} \cdot \frac{\varepsilon_{air} - \varepsilon_{eff}}{\varepsilon_{eff} + L(\varepsilon_{air} - \varepsilon_{eff})} = 0 \quad \text{(S5)}$$

Here, f_m and f_{air} (= 1 - f_m) are the volume fractions of metal and air (or void) in inhomogeneous metal film, respectively and ε_m and ε_{air} (= 1) are dielectric functions of metal and air,

respectively. L is the depolarization factor where in BEMT, it is identical to the critical filling factor at the percolation threshold [19] in which approximated as 0.59 for our case. Dielectric function of void-free 13 nm thick Ag (Cu) film was chosen as ε_m in the calculation. Thickness of Ag (Cu) film was varied from 13 nm down to 2 nm and its measured real part of dielectric function ε_1 is plotted as solid lines in **Figure S10**. Top-down TEM images for each given film thickness are shown on the inset from which the projected air fraction ϕ_{air} (ranging from ranging from 0 to 48.3 ± 4.7 %) were calculated. Note there is a minute change in ε_1 at the visible to near-infrared wavelength range when the thickness of the film is reduced from 13 nm to 8.5 nm as long as the air fraction portion is negligible. It is around the thickness of 5 nm or below at which ε_1 dramatically changes, which indicates that ε_1 is strongly influenced by ϕ_{air} as air fraction portion becomes substantial. BEMT model (**Equation S5**) was used to calculate ε_{eff} to fit the measured ε_1 by using f_{air} as a fitting parameter. As the model does not consider loss terms, only the real part dielectric function was considered. The modeled ε_{eff} are plotted as dotted lines in Figure S10 and corresponding f_{air} values are labeled. Interestingly, ε_{eff} from BEMT model well follows the curve of measured dielectric function while f_{air} values reflecting the actual film's air void fraction ϕ_{air}. As the result indicates, evolution of optical property in our Ag (Cu) film near critical thickness d_c is well approximated by EMA which further indicates inhomogeneity of metal film as the possible cause of increasing film's resistivity.

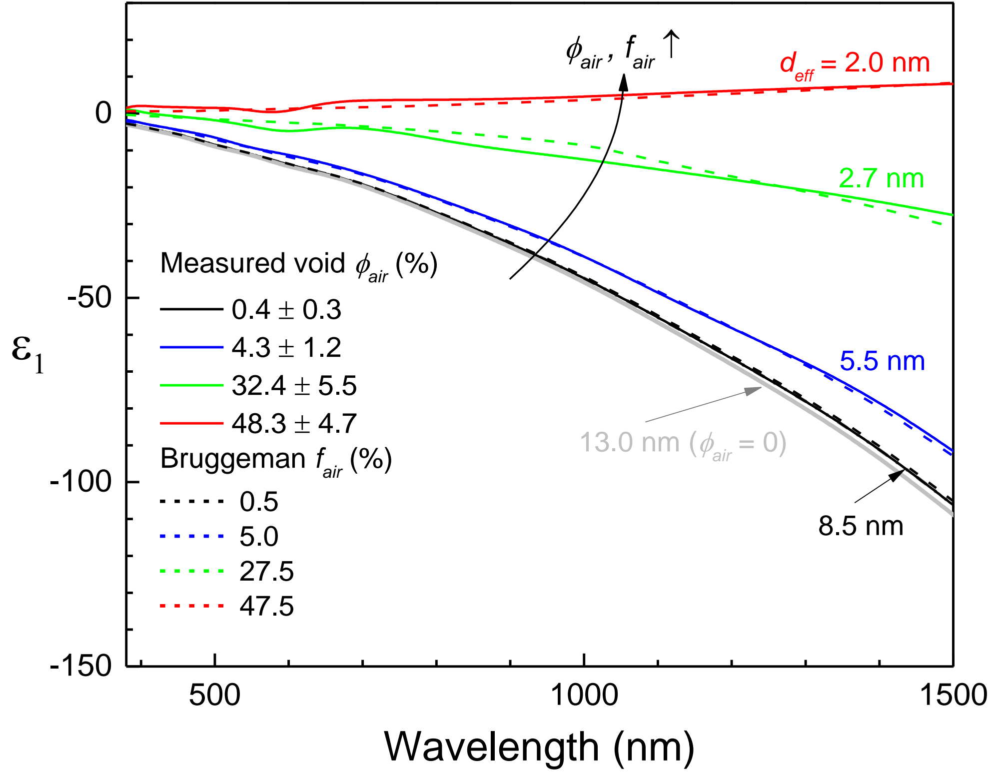

Figure S10 | Ag (Cu) film's real part of dielectric function ε_1 as a function of wavelength for different air fraction. Solid lines are the measured ε_1 for varying projected air fraction ϕ_{air}. Dashed curves are ε_1 (real part of ε_{eff}) calculated from BEMT model [Equation S5] for varying volumetric air fraction f_{air}. For each curve, corresponding film thickness d_{eff} are noted as well. The curves show a trend of increase in ε_1 for entire wavelength range as air fraction increases.

SECTION 8 | Electrical properties of Ag (Cu) film near the critical thickness

Below critical thickness d_c (solid black vertical line), Ag (Cu) film's electrical property undergoes a drastic change. **Figure S11a** shows the measured mobility μ and free carrier concentration N_c as a function of d_{eff} where μ rapidly drops below d_c while N_c remains unchanged. As both terms determine the resistivity ρ $(= 1/q\mu N_c)$, rapid increase in the resistivity below d_c is attributed to the mobility decrease by increased scattering rate as discussed in the main text. Next, **Figure S11b** shows measured (symbol) and theoretical (dashed line) scattering time τ as well as the product of resistivity and film thickness ($\rho \times d_{eff}$), all plotted as a function of d_{eff}. As already discussed in the main text, electron's scattering time

rapidly diminishes for thickness below d_c which is also predicted by the extended GEM model. Interestingly, this critical thickness is identical to the thickness that satisfies the minimum $\rho \times d_{eff}$, which is consistent with the transition thickness discussed by Vancea et al. [20]

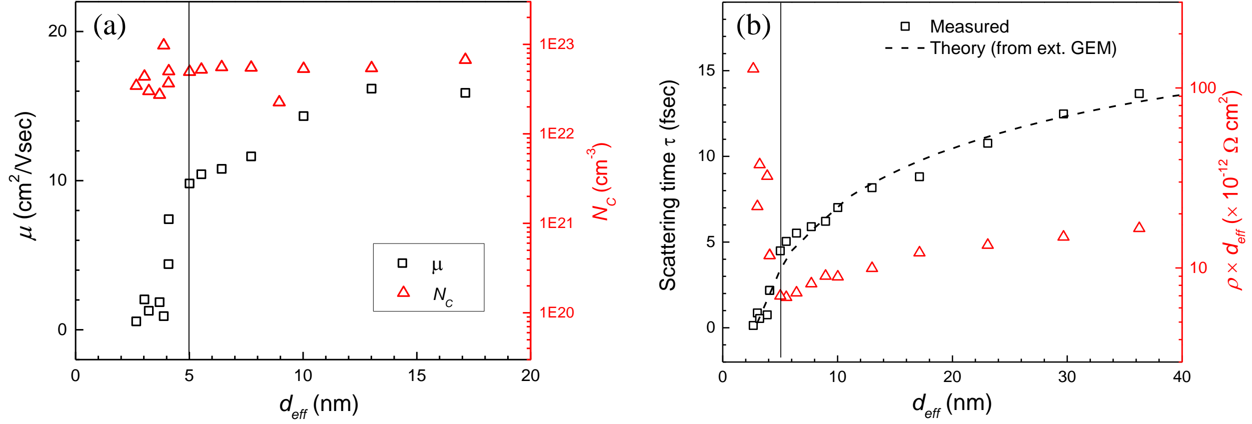

Figure S11 | Ag (Cu) film's (a) mobility μ, carrier concentration N_c, (b) scattering time τ, and $\rho \times d_{eff}$ plotted as functions of film's effective thickness d_{eff}. Solid black lines in each figure indicates the critical thickness d_c. Dashed line in (b) shows theoretical τ calculated from extended GEM model [Equation 2 from the main text].

SECTION 9 | Film's electrical hysteresis over time

Hysteresis in resistivity is observed over a span of time for metal films with thickness below d_c. For practical application, the stability of Ag thin film's electrical property is a crucial factor to consider. In this aspect, **Figure S12** plots the percentage change in the resistivity of a film after exposure in air for 30 days. The films measured undergo an increase in the resistivity after exposure in air though the degree of change is different for each thickness. For a thickness below d_c, the hysteresis in resistivity tend to increase especially near the percolation threshold. One possible explanation is that the quasi-film like morphology can be impervious to the resistivity increase. This is because unlike a continuous film where the oxide formed on the surface is parallel to the applied electric field direction, metal clusters in quasi-film has surface not only parallel but also perpendicular to the field therefore significantly impede the applied field. The effect of metal fraction ratio in the hysteresis of resistivity was tested by Sieradzki et al. where they observed larger increase in the resistivity of the film with low area coverage of metal after annealing at high temperature. [21]

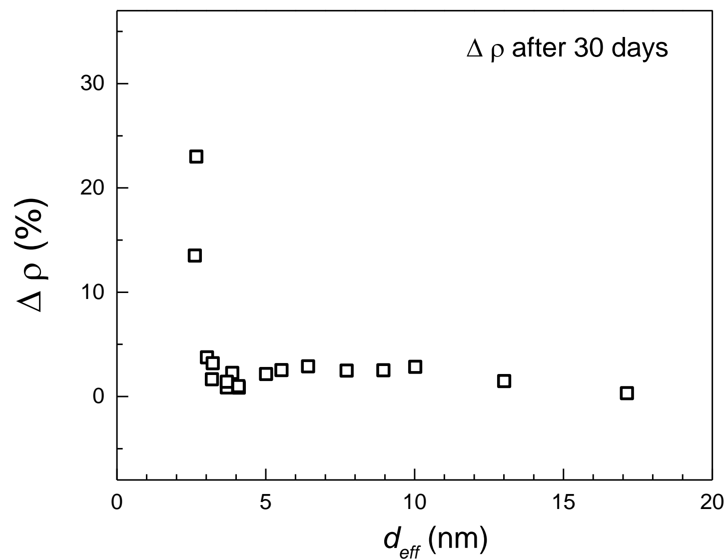

Figure S12 | Change in resistivity $\Delta\rho$ of Ag (Cu) film for different d_{eff} after exposure in air for 30 days.

References

[1] A. F. Mayadas, R. Feder, R. Rosenberg, Journal of Vacuum Science and Technology 1969, 6, 690.

[2] D. Gall, Journal of Applied Physics 2016, 119, 085101.

[3] S. B. Soffer, Journal of Applied Physics 1967, 38, 1710.

[4] Y. Namba, Japanese Journal of Applied Physics 1970, 9, 1326.

[5] K. N. Tu, A. M. Gusak, I. Sobchenko, Physical Review B 2003, 67, 245408.

[6] E. H. Sondheimer, Advances in Physics 1952, 1, 1.

[7] T. Sun, B. Yao, A. P. Warren, K. Barmak, M. F. Toney, R. E. Peale, K. R. Coffey, Physical Review B 2010, 81, 155454.

[8] J. S. Chawla, F. Gstrein, K. P. O'Brien, J. S. Clarke, D. Gall, Physical Review B 2011, 84, 235423.

[9] M. B. Heaney, Physical Review B 1995, 52, 12477.

[10] M. Taya, *Electronic Composites: Modeling, Characterization, Processing, and MEMS Applications*, Cambridge University Press, 2005.

[11] M. Hövel, B. Gompf, M. Dressel, Physical Review B 2010, 81, 035402.

[12] S.-I. Lee, Y. Song, T. W. Noh, X.-D. Chen, J. R. Gaines, Physical Review B 1986, 34, 6719.

[13] F. Carmona, A. El Amarti, Physical Review B 1987, 35, 3284.

[14] S. Mertens, C. Moore, Physical Review E 2012, 86, 061109.

[15] B. Abeles, H. L. Pinch, J. I. Gittleman, Physical Review Letters 1975, 35, 247.

[16] E. Dobierzewska-Mozrzymas, P. Biegański, E. Pieciul, J. Wójcik, Vacuum 1997, 48, 293.

[17] R. Landauer, J. C. Garland, D. B. Tanner, AIP Conference Proceedings 1978, 40, 2.

[18] D. E. Aspnes, Thin Solid Films 1982, 89, 249.

[19] T. C. Choy, *Effective Medium Theory: Principles and Applications*, Clarendon Press, 1999.

[20] J. Vancea, H. Hoffmann, K. Kastner, Thin Solid Films 1984, 121, 201.

[21] K. Sieradzki, K. Bailey, T. L. Alford, Applied Physics Letters 2001, 79, 3401.